SANDIA REPORT
SAND2011-8082
Unlimited Release
Printed September 2011

Comparison of Binary Collision Approximation and Molecular Dynamics for Displacement Cascades in GaAs

Stephen M. Foiles

Prepared by
Sandia National Laboratories
Albuquerque, New Mexico 87185 and Livermore, California 94550

Sandia National Laboratories is a multi-program laboratory managed and operated by Sandia Corporation, a wholly owned subsidiary of Lockheed Martin Corporation, for the U.S. Department of Energy's National Nuclear Security Administration under contract DE-AC04-94AL85000.

Issued by Sandia National Laboratories, operated for the United States Department of Energy by Sandia Corporation.

Available to DOE and DOE contractors from
U.S. Department of Energy
Office of Scientific and Technical Information
P.O. Box 62
Oak Ridge, TN 37831

Telephone: (865) 576-8401
Facsimile: (865) 576-5728
E-Mail: reports@adonis.osti.gov
Online ordering: http://www.osti.gov/bridge

Available to the public from
U.S. Department of Commerce
National Technical Information Service
5285 Port Royal Rd.
Springfield, VA 22161

Telephone: (800) 553-6847
Facsimile: (703) 605-6900
E-Mail: orders@ntis.fedworld.gov
Online order: http://www.ntis.gov/help/ordermethods.asp?loc=7-4-0#online

SAND2011-8082
Unlimited Release
Printed October 2011

Comparison of Binary Collision Approximation and Molecular Dynamics for Displacement Cascades in GaAs

Stephen M. Foiles
Computational Materials Science and Engineering Department

Sandia National Laboratories
P.O. Box 5800
Albuquerque, New Mexico 87185-1411

ABSTRACT

The predictions of binary collision approximation (BCA) and molecular dynamics (MD) simulations of displacement cascades in GaAs are compared. There are three issues addressed in this work. The first is the optimal choice of the effective displacement threshold to use in the BCA calculations to obtain the best agreement with MD results. Second, the spatial correlations of point defects are compared. This is related to the level of clustering that occurs for different types of radiation. Finally, the size and structure of amorphous zones seen in the MD simulations is summarized. BCA simulations are not able to predict the formation of amorphous material.

ACKNOWLEDGMENTS

Phillip Cooper of the Applied Nuclear Technologies Department at Sandia National Laboratories performed the BCA results presented in this report.

CONTENTS

FIGURES

TABLES

NOMENCLATURE

MD	Moelcular Dynamics
BCA	Binary Collision Approximation
EAM	Embedded Atom Method
LAMMPS	Large-scale Atomistic Molecular Massively Parallel Simulator
DOE	Department of Energy
SNL	Sandia National Laboratories

1. Introduction

The Binary Collision Approximations (BCA) [1] is the standard technique for the efficient computation of the primary damage produced by radiation damage. As the name implies, the full atomic dynamics of a material is approximated by a series of binary collisions. This produces a cascade of displacements that proceed until all of the atoms have recoil energies low enough that they no longer move. A consequence of the BCA approach is that all initial damage is produced via the formation of Frenkel pairs, i.e. a vacancy and an interstitial. This approximation is felt to be reasonable for high-energy recoils where the energetics of the crystalline bonding is small compared to the recoil energy of the atoms.

Molecular dynamics (MD) simulations are an alternative to BCA methods. MD simulations follow the complete atomic-level dynamics of the system based on a representation of the interatomic interactions. MD simulations have the advantage that they do not assume the nature of the defects that are formed. The atomic motion simply results from the forces during the radiation event. Further, if the interatomic interaction provides a good representation of the crystalline bonding, MD simulations will provide a reasonable description of the defect formation processes when the recoil energies are comparable to the bonding energies in the lattice such as occurs at end-of-range. The MD and BCA methods have been reviewed and compared by Robinson [2] and by Averback and Diaz de la Rubia [3].

One of the crucial parameters associated with primary damage production is the threshold displacement energy, E_d. E_d is defined as the minimum recoil energy of a given ion that will produce damage in the lattice. This value can be determined experimentally. The basic idea is to irradiate the sample, typically with electron radiation, and then look for a signature of point defect production. The energy of the radiation is varied to determine the lowest energy that produces defects. This energy is then converted to the maximum energy transferred to the recoiling particle to obtain the threshold displacement energy. It should be noted that the fraction of recoils of an energy, E, that produce damage increases from zero at the threshold energy and should saturate near unity for high-energy recoils. This reflects both the dependence of the recoil event on the direction of the recoil and stochastic factors associated with, for example, thermal vibrations.

In the context of BCA calculations, one of the input parameters is the effective threshold displacement energy, $E_{d,eff}$. In the typical implementation of the BCA, it is assumed that if an ion is given an impulse with a recoil energy $E < E_{d,eff}$ that it will not produce damage while for $E > E_{d,eff}$ there will be damage produced. Thus the smooth increase of the fraction of recoils producing damage is modeled by a step function. It is expected that the most physical choice of $E_{d,eff}$ will be above E_d.

The goals of the present work MD simulations are three-fold. The first is to estimate the best value of $E_{d,eff}$ to use in BCA calculations. This will involve detailed comparisons between the predictions of MD and BCA calculations. The second goal is to compare the spatial distribution of defects as predicted by MD and BCA calculations. The third and final goal is to provide preliminary information on the formation of amorphous zones in displacement cascades. The

formation of amorphous zones can be inferred from the results of MD simulations, but cannot be addressed with BCA calculations.

2. Methodology

2.1. Interatomic Potentials

The development of an interatomic potential for GaAs is challenging for a variety of reasons. Due to the covalent nature of the bonding, the interatomic interactions will, at a minimum, depend on both bond distances and bond angles. In this sense, the challenge is similar to elemental covalent solids such as silicon. The presence of two species means that there are more types of interactions that must be considered compared to an elemental material. This makes the fitting problem larger and significantly increases the database required to optimize the interaction model. Further, there is the possibility of some level of ionic character in the interactions. The potentials discussed below do not consider this explicitly.

There are three existing interatomic potential models for GaAs based on extensions of the functional form proposed by Tersoff for the modeling of Si and other covalent systems [4]. The first such potential was developed by Smith [5]. This parameterization was later modified by Sayed [6]. Studies with these potentials showed that they have significant short-comings with regard to surfaces, melting behavior, point defect properties and relative energies of alternate crystal structures [7]. For these reasons, the potentials are not viewed as reliable for defect simulations. More recently, a new parameterization of the Tersoff approach was performed by Albe, Nordlund, Nord and Kuronen (ANNK) [8]. The strengths and weaknesses of the above potentials for GaAs have been analyzed and discussed in the context of vapor phase deposition by Murdick, Zhou and Wadley [9].

Recently, a new potential model for GaAs has been proposed [10] which is based on the analytic Bond-Order-Potentials (BOP) that have been pioneered by Pettifor and coworkers [11-16]. The bond-order potentials are based on a tight-binding description of the electronic bonding in sp-valent systems. The analytic forms are developed to describe both the σ- and π-type bonding for systems that form open phases, close-packed structures and compounds. The details of the application of BOP to the sp-valent materials is discussed in detail by Drautz, et al. [11] and the details of the specific potential employed here are presented by Murdick, et al. [10] as well as the values of various point defects in GaAs. While the physical motivation behind the BOP potentials is superior to the Tersoff potentials, the computational effort associated with these potentials is also substantially greater.

2.2. Molecular Dynamics Simulations

The basic approach for simulating displacement cascades has been established for many years and has been reviewed by Averback and de la Rubia [3]. In the current study, the focus is on neutron damage. Imparting an impulse to a single ion and then following the evolution of the system simulates the interaction of the neutron with the ions. Recoil energies ranging from a few eV up to 50 keV are considered in this study. The simulations were performed using the LAMMPS [17] molecular dynamics program with a parallel implementation of the BOP potentials. The variable time step algorithm was used so that the maximum displacement of an atom in a given time step is less than 0.01 Å and the time step is always less than 1 femtosecond.

The length of each simulation is approximately 10 ps. Since data is output at fixed intervals in units of time steps, the variable time step means that there is some variation in the duration of different simulations. The initial state is an ideal GaAs lattice thermalized at 300 K in a cell with periodic boundary conditions. The size of the system used depended on the recoil energy. For the 50 keV simulations, the simulation cell contained 13, 824, 000 atoms corresponding to a cell side of 120 lattice constants or about 68 nm. A Langevin thermostat is applied to the atoms in the vicinity of the periodic boundaries. The recoiling atom and recoil direction are chosen so that the cascade will occur within the unthermostatted region. The Langevin thermostat serves two purposes. First, it maintains the overall system temperature near 300 K. This is a modest effect since the system sizes used are such that the temperature gain from the recoil energy would only be a few 10's of degrees. The other influence of the Langevin thermostat is to disrupt the pressure waves produced by the recoil event as they pass through the periodic boundary conditions and back into the region of the initial recoil.

2.3. Defect Analysis

A significant challenge in the analysis of displacement cascades is the identification of the defects that are produced. Recall that MD simulations produce a large set of atomic coordinates. What is desired is information about the nature of the resulting structures including the number and spatial distribution of various types of defects that are produced. This requires an analysis of the atomic positions resulting from the cascade dynamics. There have been many methods used in the past to identify defects in cascade simulations. These methods have looked at the local potential energy of atoms [18, 19], bond angles [20, 21] and radial distribution functions [19, 22]. Other approaches consider the occupation of cells surrounding ideal lattice sites as has been reviewed by Nordlund et al. [23].

The present work employs a generalization of an approach used in an earlier study of Si [24]. The defect analysis is inherently more complicated for an ordered binary alloy compared to an elemental semiconductor due to the need to consider two types each of vacancies and interstitials in addition to the new possibility of anti-site defects. A key feature of this approach is that the regions in the vicinity of the cascade are categorized as either amorphous or crystalline. The crystalline regions will potentially include point defects. The rationale for this approach is that different types of structural analysis methods make sense in these two regimes. For example, it is problematic to define point defects, such as an interstitial, in an amorphous region.

The criteria used to differentiate the amorphous and crystalline regions are the presence of 5- and 7-member rings. A ring is defined here to be a path of nearest neighbor atomic sites that returns to the original site. For this analysis, the elemental type of the atoms in the path are ignored, though in the ideal structure the atomic types should alternate around the ring. In an ideal diamond structure lattice the smallest rings are paths of 6- and 8-members or hops. It has been established that in amorphous Si and other systems that form a diamond structure that there is a significant presence of 5- and 7-member rings. The first step of the analysis is to identify all rings of 7 members or less. The cell is then subdivided into regions the size of the cubic unit cell of the GaAs lattice and the number of 5- and 7-member rings centered in each cell is counted. Cells that contain more than one 5-member ring or more than two 7-member rings are classified as amorphous regions. The remainder of the system is classified as crystalline.

The crystalline regions are then analyzed for point defects using a cell based method similar to the methods reviewed by Nordlund et al [23]. An ideal GaAs lattice is constructed and shifted so as to optimize the overall alignment of the ideal lattice with the atomic positions from the MD simulations. Space-filling cells are considered around each of the ideal lattice sites and the occupation of each such cell is determined. Point defects are identified with those cells that do not contain one and only one atom of the appropriate type. The initial assignment of defect types follows in an obvious manner. A cell with no atoms corresponds to a vacancy. The vacancies are further identified as Ga-vacancies and As-vacancies based on the atomic species that would occupy that ideal lattice site. A site with multiple atoms corresponds to an interstitial. The type of the additional atom determines whether the site is a Ga- and As-interstitial. Finally, a cell with one atom but of the wrong type corresponds to an anti-site defect. A Ga anti-site defect refers to a Ga atom located in an As cell.

The point defects so produced are next combined with defects on neighboring sites as appropriate. There are two reasons for such combinations. First, it is expected that certain nearest neighbor defect pairs will heal rapidly. For example an interstitial adjacent to a vacancy would be expected to annihilate quickly. Second, such combination of defects is consistent with the typical analysis of binary collision calculations. The inclusion of near-neighbor defect combination therefore facilitates the comparison with BCA results. The following nearest neighbor pairs of defects are combined: vacancy and interstitial of the same type annihilate, a vacancy and an interstitial of the opposite type form a anti-site defect of the type of the interstitial, a vacancy and a neighboring anti-site for a vacancy of the opposite type on the initial site of the anti-site defect. The process of combining defects is repeated until the resulting defect configuration is stable.

3. Effective Threshold Energy

Simulations were performed to determine the threshold displacement energy associated with the BOP potentials used here. These simulations used a simulation cell of 32, 768 atoms at ideal lattice sites with the atoms at ideal lattice sites. At each energy a series of simulations with an atom given that recoil energy are performed. A grid of recoil directions is chosen so as to uniformly sample the solid angle of the recoil directions. The trajectory is then computed for each direction and the defect analysis described above is performed to determine if there are defects produced. Figure 1 presents the fraction of directions that produced defects as a function of energy for both Ga and As recoils. For both species, no recoils were observed for simulations at 10 eV or below while a small number of recoils are observed at 11 eV. For both species, the recoils that produce damage at threshold are along <111>, ie along the nearest neighbor directions. The fraction of recoils that produce damage increases rapidly with energy until is starts to approach unity for recoils up to 100 eV. The energy at which about half of the recoils produce damage is around 20eV. Note that there is at most a small difference between the results for Ga and As recoils. The fraction of Ga recoils that produce persistent defects appears to be somewhat lower than for As recoils, but this effect is small compared to the error bars. The similarity of the results for the two types of recoils is not surprising given the similar mass, short-range repulsion and covalent radii of the two elements. It is anticipated that for systems with greater differences in these properties, that there would be significant differences in the threshold energies for the differing ions.

There have been several experimental studies of the displacement energy in GaAs. Some of the reported threshold energies, in chronological order, are 9 eV [25], 17-18 eV [26], 9-10 eV [27, 28], and10.0±0.7 eV [29] and 9 eV [30]. The threshold displacement energy has been discussed in a review by Pons and Bourgoin [31] and a recent compilation of displacement energies lists 10 eV [32]. An important observation regarding the low-energy defect formation energy is the anisotropy of the defect production with the direction of the electron irradiation in single crystal samples [27, 30, 33, 34]. It is observed that the damage production occurs when the electron irradiation is in the [111] direction, ie along the nearest neighbor directions of the lattice.

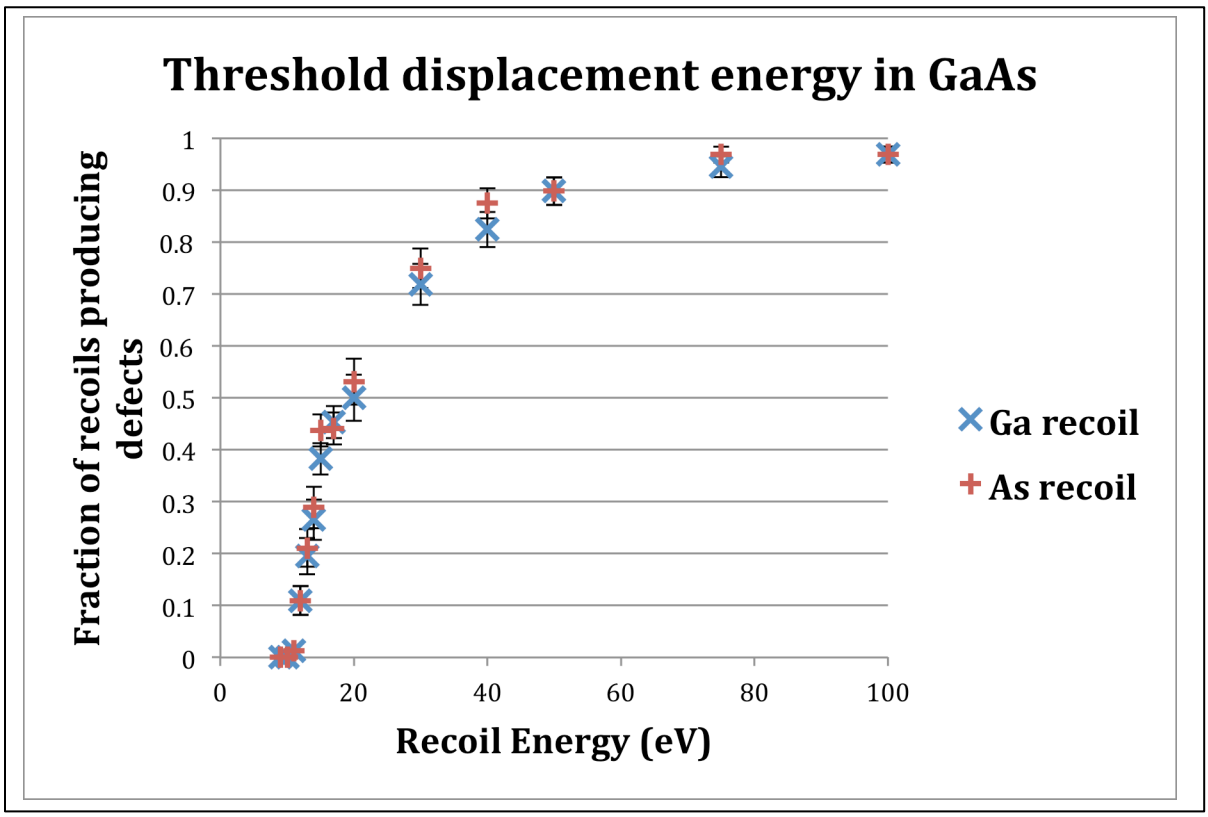

Figure 1. The fraction of MD simulations that produced persistent damage as a function of the recoil energy for both Ga (x) and As (+) recoils.

The results shown in Figure 1 allow for the determination of the threshold energy of E_d = 11 eV. This is the lowest energy for which persistent damage is observed in the MD simulations. The recoils that produce damage at the threshold have a recoil direction in the <1 1 1> directions, ie parallel to the nearest neighbor bonds in the GaAs crystal. Note that there is at most a small difference between the results for Ga and As recoils. The fraction of Ga recoils that produce persistent defects appears to be somewhat lower than for As recoils, but this effect is small compared to the error bars. The similarity of the results for the two types of recoils is not surprising given the similar mass, short-range repulsion and covalent radii of the two elements. It is anticipated that for systems with greater differences in these properties, that there would be significant differences in the threshold energies for the differing ions.

Given that these results are predictions, they are in satisfactory agreement with the experimental results. Experimental estimates of the threshold vary, but the most recent results quote a value of E_d = 9 eV [30]. Experimental results also indicate that the recoils at threshold are along the <1 1 1> directions consistent with the calculations. This comparison provides experimental validation of the recoil simulations based on the BOP potential. The comparison also suggests that the threshold energies predicted from MD will be systematically high by about 2 eV.

There is not an unambiguous way to go from the results presenting in Figure 1 to the effective threshold energy. There have been some approaches discussed in the literature, but the fundamental basis for these approaches is unclear. Here I will use an intuitively appealing

criterion, namely the recoil energy at which half of the recoils produce persistent damage. Given the small differences in the results for Ga and As, the average of the two types of recoils will be used. This simple criterion gives a estimate of the effective threshold energy for the MD simulations of $E_{d,eff,MD}$ = 19 eV.

The effective threshold displacement energy can also be estimated by the direct comparison of the number of defects produced in the MD and BCA calculations. In this approach, BCA calculations are performed for a variety of assumed threshold energies. The number of defects produced as a function of effective threshold energy can then be compared to the MD estimates of the defect production number. For this comparison, the number of vacancies was chosen as the measure of defect production. This comparison is done for two recoil energies, 10 keV and 50 keV.

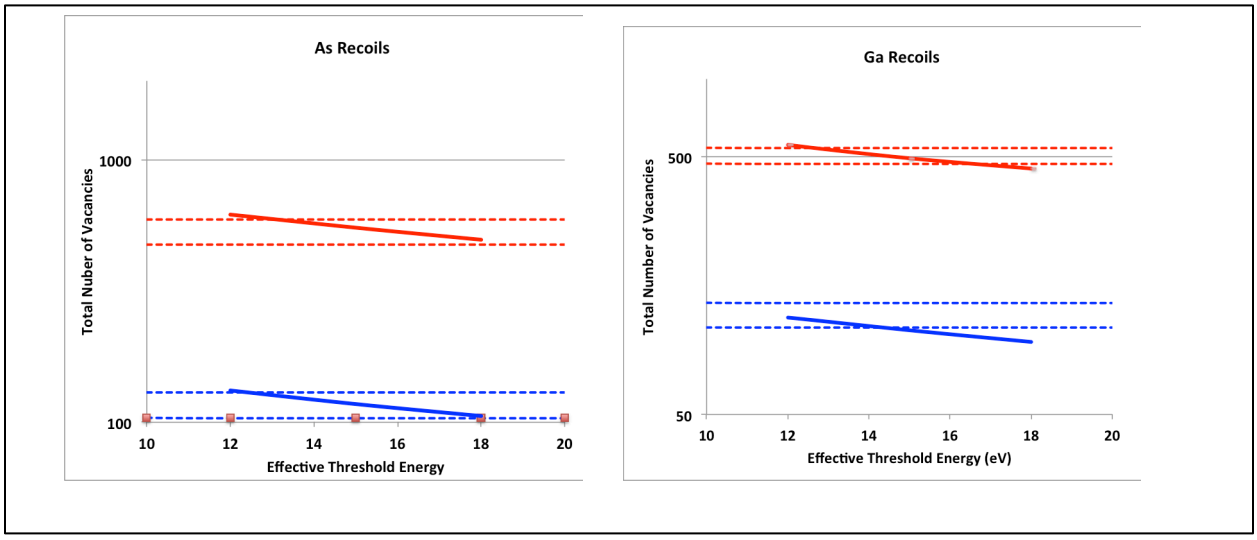

Figure 2: The horizontal dashed lines represent the range of the total number of vacancies produced in MD simulations for recoil energies of 10 keV (blue) and 50 keV (red). The range represents the mean plus or minus the standard deviation. The solid curves represent the total number of vacancies predicted by BCA calculations as a function of the effective threshold energy used in the calculation.

Figure 2 shows the resulting comparison. The horizontal lines represent the range of values for the average number of vacancies produced based on 10 MD simulations. This range is obtained by taking the mean number of vacancies produced and adding or subtracting the standard error of the mean. The wide range of possible values reflects the large variation from case to case in the number of vacancies produced. The solid lines represent the number of vacancies predicted in the BCA calculations. In this case, the number of simulations is significantly larger. Thus the statistical errors are smaller and are not included on the plots. In three of the four cases, the BCA and MD results are consistent for effective threshold energies in the range of about 14 – 16 eV. In the final case, the results are consistent for effective energies less than about 15 eV. While a precise determination of the best effective threshold energy is not possible from these results, a value of 15 eV appears to be a reasonable choice.

Having set the effective threshold energy to obtain agreement between MD and BCA for the vacancy production, it is important to compare the number of other defect types predicted by the two approaches at the same effective threshold energy. The results of this comparison are shown in the table. The predicted number of interstitials is marginally in agreement between the two approaches and there is substantial disagreement on the number of anti-site defects produced.

Recoil Type	Defect	MD 10 keV	BCA 10keV	MD 50 keV	BCA 50 keV
Ga	Ga int.	44.2 ± 1.8	52.9 ± 0.5	188.9 ± 9.6	248.2 ± 2.9
As	Ga int.	46.3 ± 2.9	58.3 ± 0.5	194.7 ± 10.3	277.8 ± 2.7
Ga	As int.	45.7 ± 4.7	50.9 ± 0.5	196.8 ± 11.2	240.1 ± 2.9
As	As int.	41.1 ± 4.3	57.4 ± 0.5	203.2 ± 11.2	271.8 ± 2.6
Ga	Ga anti-site	76.1 ± 6.4	21.8 ± 0.3	329.1 ± 18.5	102.0 ± 1.4
As	Ga anti-site	68.4 ± 5.7	23.4 ± 0.3	349.2 ± 15.0	118.8 ± 1.5
Ga	As anti-site	75.7 ± 6.0	22.7 ± 0.3	319.7 ± 19.9	109.0 ± 1.5
As	As anti-site	69.5 ± 7.0	24.3 ± 0.3	346.4 ± 15.6	124.6 ± 1.6

Table 1. Comparison of the predicted number of interstitial and anti-site defects predicted by the MD simulations and the BCA simulations with an effective threshold energy of 15 eV.

In general, the number of interstitial type defects predicted from the MD simulation is less than the number predicted by the BCA calculations. The difference is clearly outside the statistical uncertainty in the averages. With regard to the effective threshold energy, a value in the range of 20 eV reduces the number of interstitials in the BCA calculation into rough agreement with the MD results.

The more troubling disagreement between the MD and BCA results is in the number of anti-site defects. The MD simulations predict roughly three times the number of anti-site defects predicted by the BCA calculations. Adjusting the effective threshold displacement energy will not bring these two predictions into alignment. The source of this disagreement is currently unknown. It should be noted that visualization of the MD simulation data reveals the presence of a large number of anti-site defect pairs that may result from replacement sequences. The number of these anti-site pairs, though, is not sufficient to explain the discrepancy.

4. Correlations between point defects

The spatial extent of displacement cascades is another important characteristic. The spatial extent determines the degree of clustering of the point defects produced which impacts the long-time evolution of the damage population. The differences in the level of clustering of the point defects is believed to be a major contributor to the differences in the response to different types of radiation damage. For example, electron irradiation is expected to produce relatively uniform initial defect concentrations compared to neutrons and heavy ions that are expected to create initial defect populations that are highly clustered. It is therefore important the determine if the spatial extent of the displacement cascades predicted by BCA calculations are consistent with the results obtained using MD.

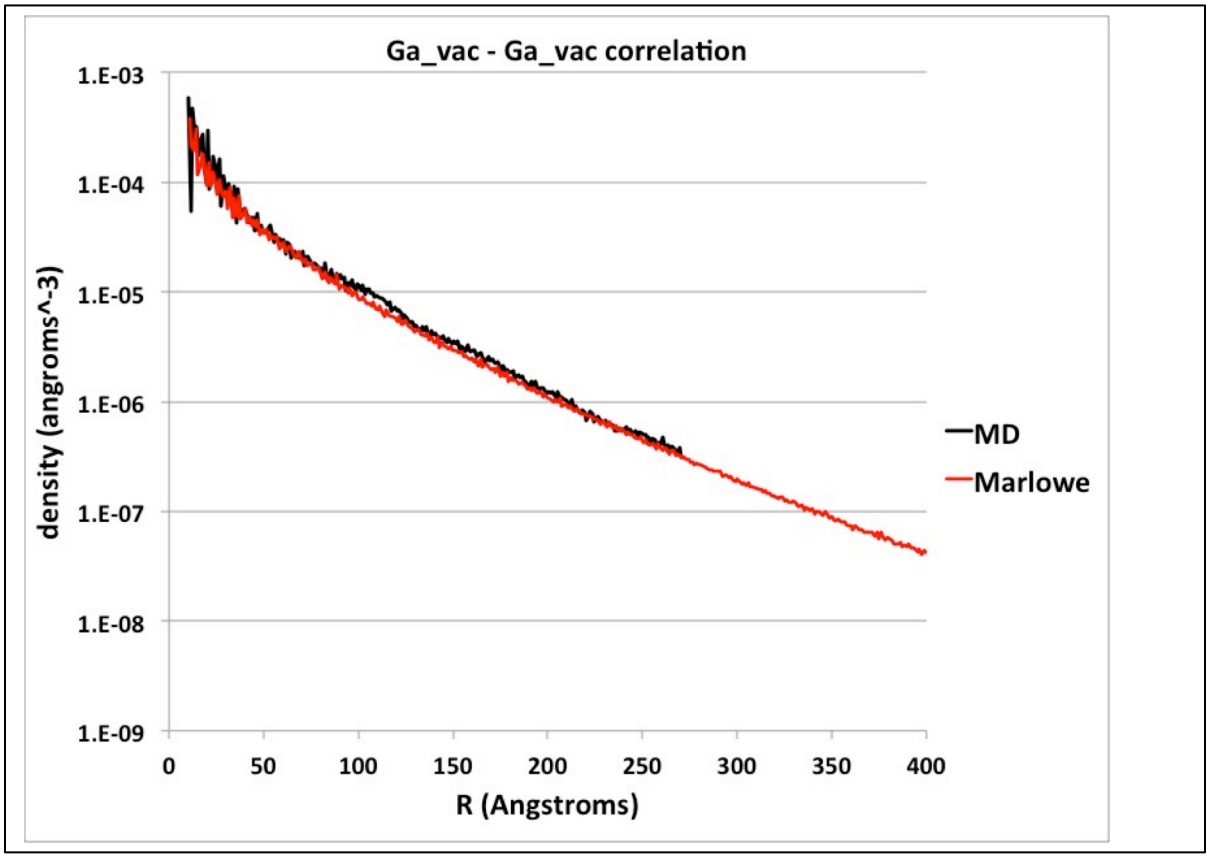

Figure 3: Correlation between Ga vacancies plotted as the density of Ga vacancies at a distance R from a Ga vacancy. The results are for 50 keV Ga recoils. The black curve are from the MD simulations and the red curve is from Marlowe (BCA) calculations assuming an effective threshold displacement energy of 15 eV.

Figure 3 presents a typical comparison of the BCA and MD results for the correlation between point defects. This results depicts the correlation function between the location of Ga vacancies. In particular, it plots the average density of Ga vacancies located at a distance R from a Ga vacancy. These results are an average over the results of simulations of 50 keV Ga recoils in GaAs. The MD results are an average over 10 simulations and are plotted in black. The BCA (Marlowe) results are an average over 500 simulations and are plotted in red. The difference in

statistical noise in the two curves reflects the difference in the number of simulations that are averaged over.

The agreement of the Ga vacancy – Ga vacancy pair correlations is very good. This indicates that the spatial distribution of the vacancies predicted by BCA and MD are in good agreement. Examination of the pair correlations between other types of defects also showed good agreement with the exception that the density values predicted by BCA and MD differed consistent with the differences in predicted defect numbers presented in Table 1. This indicates that except for the overall number of defects, the spatial distribution predictions of BCA and MD are in agreement. Thus BCA calculations can be used to assess the level of clustering in a radiation environment.

5. Amorphous Zone Production

One of the sharpest contrasts between the BCA and MD results is the prediction of amorphous regions. BCA calculations do not have a mechanism to predict amorphization, but MD simulations can predict amorphous zones. The production of amorphous zones has been observed experimentally as a result of irradiation by protons and other ions [35-39]. The production of amorphous zones has also been seen previously in molecular dynamics simulations. [22, 40] Here, the variation of the amount of amorphous material created as a function of energy will be examined. In addition, some structural characteristic of the amorphous regions will be discussed.

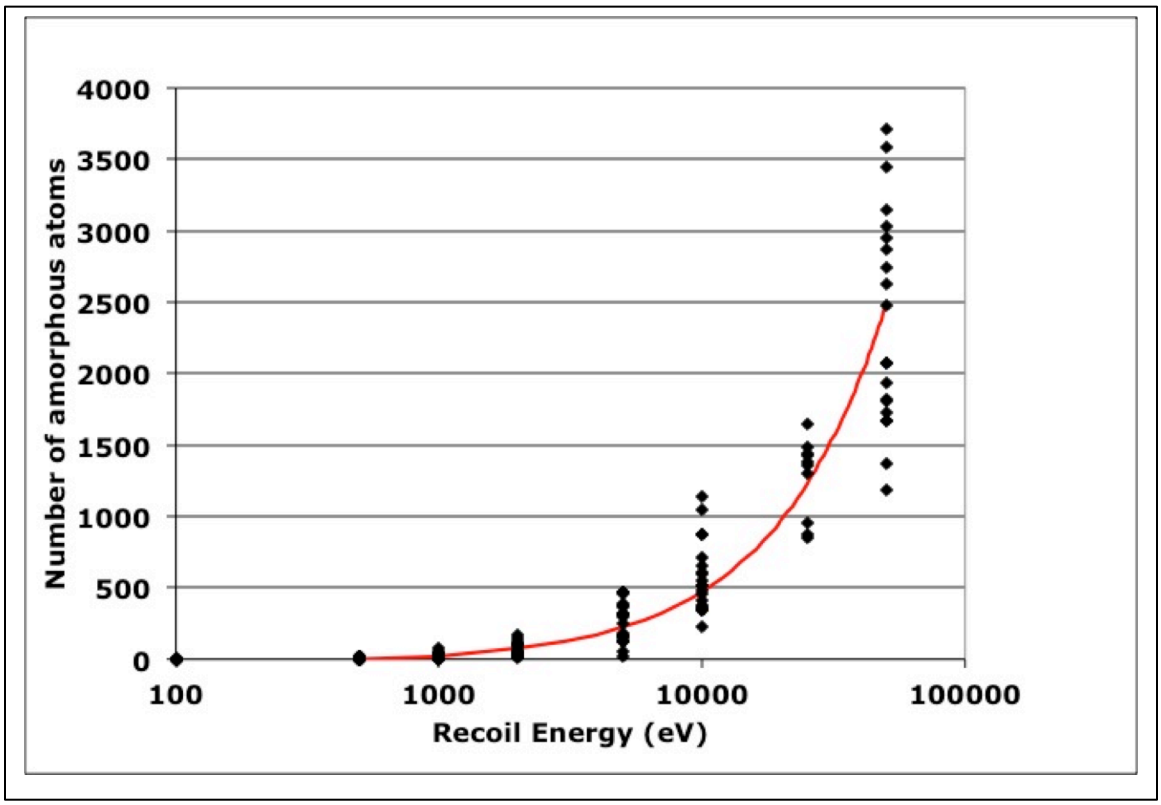

Figure 4: Number of amorphous atoms as a function of the recoil energy computed by MD simulations. The solid points reflect the results of individual simulations and the red line is a fit to the data as discussed in the text.

Figure 4 shows the number of atoms identified as amorphous by the algorithm discussed above as a function of recoil energy. Each point represents a separate simulation. In this plot, Ga and As recoils are plotted together because there was no apparent systematic difference between the two types of recoils. Note that the production of amorphous regions starts at approximately 500 eV. A similar threshold for the creation of amorphous zones was found in simulations of Si recoil cascades [24]. In the Si case, the threshold energy was in the range of 200 – 400 eV. Note that there is a wide variation in the amount of amorphous material created for recoils of the same energy; for 50 keV recoils the number of amorphous atoms varies by over a factor of 3. The solid line in the figure reflects a linear increase in the number of amorphous atoms with the

recoil energy given by $N_{amorphous} \approx 0.05(E_{recoil} - 500)$ for recoil energies in eV. This curve provides a reasonable fit to the center of the distributions at each energy. It is plausible that the average amount of amorphous material would increase linearly with energy above a threshold point. The current data is not sufficient to determine if there are better descriptions of the variation of the amount of amorphous material created as a function of recoil energy.

The coordination of the atoms in the amorphous regions has been determined by counting the number of atoms within a shell of 2.7Å around each atom in the amorphous zones. This is a distance approximately halfway between the first and second nearest neighbor distances. The results presented here are for 50 keV recoils. The results for amorphous zones in 10 keV and 25 keV recoils are not significantly different. The average coordination computed in this manner is 3.93. This is somewhat less than the value of 4 for the perfect crystal. This results is in good agreement with an experimental determination of the average coordination of amorphous GaAs by Ridgway, et al [39] that gives a value of 3.85±0.20. While the average coordination is close to 4, this does not mean that most of the atoms have the bulk coordination of 4. In these simulations, 69% of the atoms in the amorphous regions have a coordination of 4 while 15 and 13% of the atoms have coordinations of 3 and 5, respectively. Thus a significant fraction of the amorphous atoms do not have the bulk 4-fold coordination.

It is also important to consider the chemical order in the amorphous zones. In the ideal crystal, the nearest neighbor shell of each atom is comprised of atoms of the opposite chemical species. Table 2 presents a summary of the coordination and composition of atoms in the amorphous zones. The rows in the table correspond to total coordination on the amorphous atoms ranging from 2 up to 5. The columns represent the composition of the neighbor shell by indicating the number of atoms in the neighbor shell that are the same composition as the central atom. Since the results for the environments of Ga and As atoms were very similar, the results presented here are an average of the results for the neighbors of Ga and As. The individual numbers in the table represent the fraction of the amorphous atoms that have that particular neighbor environment. The results presented are for 50 keV recoils. The results for 10 and 25 keV recoils were not significantly different.

		Number of Neighbors of Same Species				
		0	1	2	3	4
Total Coordi-nation	2	0.013	0.008	0.000		
	3	0.056	0.054	0.032	0.006	
	4	0.268	0.281	0.115	0.024	0.002
	5	0.010	0.061	0.046	0.014	0.001

Table 2: Fraction of amorphous atoms with the indicated total coordination and number of neighboring atoms of the same species. These results are from MD simulations of 50 keV recoils. Atoms in an ideal crystal have a total coordination of 4 and 0 neighbors of the same species.

The most important observation is that only slightly over a quarter of the amorphous atoms have four neighbors of the opposite species as is found in the perfect crystal. A similar number have four neighbors but one of the neighbors is of the incorrect species. Thus Ga-Ga and As-As

nearest neighbors are common in the amorphous zone. These results suggest that the electronic properties of the amorphous zones may differ significantly from the ideal crystal. This will be the subject of future studies.

6. Summary

This report summarizes some comparisons between the predictions of BCA and MD simulations of displacement cascades in GaAs. In general, BCA calculations are far less computer intensive than MD simulations and are therefore the preferred method to study the damage produced by complex radiation environments. MD simulations incorporate fewer physical assumptions and so are thought to be more accurate. The overarching goal of the current work was to use MD simulations to obtain an appreciation of the reliability of BCA results.

There is not a unique value of the effective threshold energy based on these calculations. An examination of the energy dependent defect production probability and matching the number of interstitials produced both suggest an effective threshold in the range of 19-20 eV. Matching the number of vacancies produced yields an effective threshold of about 15 eV. Note that since the threshold energy predicted by the MD is about 2 eV higher than experiment, either of these estimates should be reduced by 2 eV to compare to experimental results.

The spatial correlation of point defects as predicted by the two methods was also examined. It was found that the two methods agree on the spatial distribution of the defects produced in a single cascade.

Finally, MD simulations were used to determine the local atomic structure in amorphous zones produced in high-energy recoils. BCA calculations cannot study amorphous zone formation. The average coordination predicted by the MD simulations is in accord with experimental observations. There are significant differences in the nearest neighbor environment of atoms in the amorphous zone compared to the ideal crystal. The implications of these differences on the electronic structure will be the subject of future studies.

7. References

1. Robinson, M.T. and I.M. Torrens, *Computer simulation of atomic-displacement cascades in solids in the binary-collision approximation.* Physical Review B, 1974. **9**: p. 5008.
2. Robinson, M.T., *Basic Physics of Radiation Damage Production.* Journal of Nuclear Materials, 1994. **216**: p. 1-28.
3. Averback, R.S. and T. Diaz de la Rubia, *Displacement Damage in Irradiated Metals and Semiconductors*, in *Solid State Physics: Advances in researh and Applications*, H. Ehrenreich and F. Spaepen, Editors. 1998, Academic Press: San Diego. p. 281-403.
4. Tersoff, J., *Empirical interatomic potential for silicon with improved elastic constants.* Physical Review B, 1988. **38**(14): p. 9902.
5. Smith, R., *A semi-empirical many-body interatomic potential for modelling dynamical processes in gallium arsenide.* Nuclear Instruments and Methods in Physics Research B, 1992. **67**: p. 335-339.
6. Sayed, M., et al., *Computer simulation of atomic displacements in Si, GaAs, and AlAs.* Nuclear Instruments and Methods in Physics Research B, 1995. **102**: p. 232-235.
7. Nordlund, K. and A. Kuronen, *Non-equilibrium properties of GaAs interatomic potentials.* Nuclear Instruments and Methods in Physics Research B, 1999. **159**: p. 183-186.
8. Albe, K., et al., *Modeling of compound semiconductors: Analytic bond-order potential for Ga, As and GaAs.* Physical Review B, 2002. **66**: p. 035205.
9. Murdick, D.A., X.W. Zhou, and H.N.G. Wadley, *Assessment of interatomic potentials for molecular dynamics simulations of GaAs deposition.* Physical Review B, 2005. **72**: p. 205340.
10. Murdick, D.A., et al., *Analytic bond-order potential for the gallium arsenide system.* Physical Review B, 2006. **73**: p. 045206.
11. Drautz, R., et al., *Analytic bond-order potential for predicting structural trends across the sp-valent elements.* Physical Review B, 2005. **72**: p. 144105.
12. Pettifor, D.G., *New Many-Body Potential for the Bond Order.* Physical Review Letters, 1989. **63**: p. 2480-2483.
13. Pettifor, D.G., et al., *Analytic bond-order potentials for multicomponent systems.* Materials Science and Engineering A, 2004. **365**: p. 2-13.
14. Pettifor, D.G. and I.I. Oleinik, *Analytic bond-order potentials beyond Tersoff-Brenner: Theory.* Physical Review B, 1999. **59**: p. 8487-8499.
15. Pettifor, D.G. and I.I. Oleinik, *Bounded analytic Bond-Order Potentials for sigma and pi Bonds.* Physical Review Letters, 2000. **84**: p. 4124-4127.
16. Pettifor, D.G. and I.I. Oleinik, *Analytic bond-order potentials for open and close-packed phases.* Physical Review B, 2002. **65**: p. 172103.
17. Plimpton, S.J., *LAMMPS: Large-scale Atomic/Molecular Massively Parallel Simulator*, 2007, Sandia National Laboratories.
18. Ghaly, M. and R.S. Averback, *Effect of Viscous Flow on Ion Damage near Solid Surfaces.* Physical Review Letters, 1994. **72**: p. 364.
19. Rubia, T.D.d.l. and G.H. Gilmer, *Structural Transformaations and Defect Production in Ion Implanted Silicon: A Molecular Dynamics SImulation Study.* Phys. Rev. Lett., 1995. **74**(13): p. 2507.

20. Marqués, L.A., et al., *A novel technique for the structural and energetic characterization of lattice defects in the molecular dynamics framework.* Comp. Mat. Sci., 2005. **33**: p. 112.
21. Uttormark, M.J., M.O. Thompson, and P. Clancy, *Kinetics of crystal dissolution for a Stillinger-Weber model of silicon.* Phys. Rev. B, 1993. **47**(23): p. 15717.
22. Nord, J., K. Nordlund, and J. Keinonen, *Amorphization mechanism and defect structures in ion-beam-amorphiszed Si, Ge, and GaAs.* Physical Review B, 2002. **65**: p. 165329.
23. Nordlund, K., et al., *Defect production in collision cascades in elemental semiconductors and fcc metals.* Physical Review B, 1998. **57**: p. 7556.
24. Foiles, S.M., *Detailed characterization of defect production in molecular dynamics simulations of cascades in Si.* Nuclear Instruments and Methods in Physics Research B, 2007. **255**: p. 101.
25. von Bäuerlein, R. in *International School of Physics, Radiation Damage in Solids*. 1960. Academic Press, New York.
26. Grimshaw, J.A. and P.C. Banbury, *The displacement energy in GaAs.* Proceedings of the Physical Society, 1964. **84**: p. 151-162.
27. Pons, D., *anisotropic defect introduction in n and p-GaAs by electron irradiation.* Physical Review Letters, 1983. **116B**: p. 388-393.
28. Pons, D., P.M. Mooney, and J.C. Bourgoin, *Energy dependence of deep level introduction in electron irradiated GaAs.* Journal of Applied Physics, 1980. **51**: p. 2038-2042.
29. Barry, A.L., et al., *An improved displacement damage monitor.* IEEE Transactions on Nuclear Science, 1990. **37**: p. 1726-1731.
30. Lehmann, B. and D. Braunig, *A deep-level transient spectroscopy variation for the determination of displacement threshold energies in GaAs.* Journal of Applied Physics, 1993. **73**: p. 2781-2785.
31. Pons, D. and J.C. Bourgoin, *Irradiation-induced defects in GaAs.* Journal of Phyics C: Solid State Physics, 1985. **18**: p. 3839-3871.
32. Averback, R.S. and M. Ghal, *Fundamental Aspects of defect production in solids.* Nucl. Instr. and Meth. B, 1997. **127/128**: p. 1-11.
33. Pons, D., *Anisotropy of defect introduction by electron irradiation in compound semiconductors.* Journal of Applied Physics, 1984. **55**: p. 2839-2846.
34. Pons, D. and J.C. Bourgoin, *Anisotropic-Defect Introduction in GaAs by Electron Irradiation.* Physical Review Letters, 1981. **47**: p. 1293-1296.
35. Bench, M.W., et al., *Production of amorphous zones in GaAs by the direct impact of energetic heavy ions.* Journal of Applied Physics, 2000. **87**: p. 49-56.
36. Ridgway, M.C., et al., *Characterization of the local struc ture of amorphous GaAs produced by ion implantation.* Journal of Applied Physics, 1998. **83**: p. 4610-4614.
37. Warner, J.H., et al., *Effect of Proton and Silicon Ion Irradiation on Defect Formation in GaAs.* IEEE Transactions on Nuclear Science, 2008. **55**: p. 3016-3024.
38. Zollo, G., *XHRTEM observations of different damage structures in high temperature Zn^{+} implanted GaAs.* Vacuum, 2003. **69**: p. 97-101.
39. Ridgway, M.C., et al., *Atomic-level characterizaion of ion-induced amorphisation in compound semiconductors.* Nuclear Instruments and Methods in Physics Research B, 1999. **148**: p. 391-395.

40. Björkas, C., et al., *Damage production in GaAs and GaAsN induced by light and heavy ions.* Journal of Applied Physics, 2006. **100**: p. 053516.

8. Distribution

1	MS1056	William Wampler	1111
1	MS1146	Philip Cooper	1384
1	MS1146	Patrick Griffiths	1384
1	MS1179	Leonard Lorence	1340
1	MS1411	Stephen Foiles	1814
1	MS0899	RIM-Reports Management	9532 (electronic copy)


Sandia National Laboratories